Available online at www.sciencedirect.com
ScienceDirect
Trans. Nonferrous Met. Soc. China 24(2014) 2559−2565
Transactions of Nonferrous Metals Society of China
www.tnmsc.cn

Microstructures of TiN, TiAlN and TiAlVN coatings on AISI M2 steel deposited by magnetron reactive sputtering

Cui-feng WANG[1], Shih-fu OU[2], Shi-yung CHIOU[2]

1. Department of Mechanical and Electrical Engineering, Fujian Polytechnic of Information Technology, Fuzhou 350003, China;
2. Department of Mold and Die Engineering, National Kaohsiung University of Applied Science, Kaohsiung 80706

Received 28 October 2013; accepted 25 February 2014

Abstract: In order to study the effect of the microstructure with Al and V added TiN coatings, TiN, TiAlN and TiAlVN coatings were deposited on AISI M2 high-speed steels by magnetron reactive sputtering. The microstructures of all the coatings were characterized by X-ray diffraction (XRD), scanning electron microscopy (SEM) and transmission electron microscopy (TEM). The results indicate that the addition of Al into TiN coatings reduces their lattice constant, but a further addition of V into TiAlN coatings increases their lattice constant. Moreover, the growth morphologies for TiN, TiAlN, and TiAlVN indicate that adding Al and V has a tendency to improve the columnar structure. The (111) and (200) orientations of TiN, TiAlN, and TiAlVN are identified. The $\varepsilon(Fe_3N{-}Fe_2N)$ phase occurs because a small amount of Fe is present in the coatings. The interlayers of TiAlN and TiAlVN have the preferred $(01\bar{1}0)$ orientation. The texture (columnar) structure of the (111) and (200) orientations is observed in the TiAlN and TiAlVN coatings. An orientation relationship of $(01\bar{1}0)_{\alpha\text{-Ti}}//(110)_{\text{T.M}}$ occurs between the interlayer and tempered martensite (T.M) in TiAlVN.

Key words: coating; TiAlVN coating; sputtering yield; crystallographic relationship

1 Introduction

Nitride coatings of transition metals are commonly used in the tribological [1−3], decorative, and biomedical applications [4] because of their high hardness, high abrasion resistance and attractive golden-yellow color. However, TiN coatings oxidize rapidly at temperatures above 500 °C and form a layer of rutile TiO_2, which determines the limit of their high-temperature applications. The large difference between the molar volumes of TiO_2 and TiN causes stress in the oxide. Its magnitude increases with increasing oxide thickness till the critical thickness, which occurs when the oxide spalls and the unoxidized nitride below is exposed to further oxidation. Further improvements in properties can be realized in multicomponent Ti-based nitride coatings. For example, TiAlN coatings on tool steels are demonstrated to have excellent high-temperature stability and abrasion resistance [5−8]. TiAlN coatings have been deposited on tool steels by magnetron sputter ion plating [9], and physical vapor deposition (PVD) [10−12].

Although TiAlN hard coatings show successful performance because of their excellent wear and thermal resistance compared with TiN coatings, a low coefficient of friction or self-lubrication properties for high-speed and dry abrasive applications is required. The addition of V as a TiAlVN multicomponent or TiAlN/VN multilayer structure [13−16] is becoming an alternate option for high-temperature use. However, the effects of V addition on the basic crystalline structure and growth morphology are not investigated although some researches about the applications of TiAlVN coatings are found.

In this study, TiN, TiAlN and TiAlVN coatings were deposited by magnetron reactively sputtered on steels from targets of pure Ti, Ti−6Al (6%) and Ti−6Al−4V (6% and 4%). The effects of Al and V on the microstructure of TiN coatings were investigated.

2 Experimental

2.1 Deposition process

AISI M2 high-speed steels used as substrates were quenched and tempered before deposition. The hardness

Corresponding author: Cui-feng WANG; Tel: +86-13609502462; E-mail: cfeng07 @126.com
DOI: 10.1016/S1003-6326(14)63383-5

of the tempered M2 is HV 780 (HRC 63). Deposition processes were undertaken using the sputtering system of CSU550-1, Shengyang Piotech Co., Ltd.. Three materials were used as targets in this study: Ti, Ti−6Al and Ti−6Al−4V. The discharge power was controlled to be 220 W and the substrate temperature was kept at 300 °C. The argon and nitrogen flow rates during deposition were 28 and 3 mL/min, respectively, with a specific ratio of 9.3. The working pressure of the chamber was maintained at 0.8 Pa. Pre-sputtering was performed by plasma for 15 min to clean the target surface. The deposition duration for growing the films to approximately 2 μm in thickness was 1 h, but the metallic interlayer was grown within the initial 5 min.

2.2 Micro-Vickers hardness testing

The surface hardness of the nitride layers was measured using a micro-Vickers hardness tester with 0.147 N load and 10 s load-holding time (Mitutoyo, MVK-H1).

2.3 Microstructure characterization

The cross-sections of each nitride film were examined using an SEM (JEOL 6400) through backscattered electron images (BEI) and secondary electron images (SEI) to identify their columnar structure. The microstructure of the coatings was analyzed by X-ray diffraction (XRD, Siemens D5000) using Cu K_{α} radiation operated at 30 kV and 25 mA, with a scanning speed of 1.5 (°)/min. Moreover, the microstructure was investigated by a transmission electron microscope (TEM, JEOL JEM−3010, operating at 300 kV).

3 Results

3.1 Micro-Vickers hardness

The micro-Vickers hardnesses are HV1560, HV1640 and HV1690 for TiN, TiAlN and TiAlVN coating on M2, respectively.

3.2 XRD

The major phases of the nitride coatings on M2 identified by XRD are shown in Fig. 1. Figure 1(a) shows the strong (111) and (200) TiN peaks and several weak peaks, which were possibly caused by the ε(Fe_3N−Fe_2N) phase or Fe by Joint Committee on Powder Diffraction Standards (JCPDS) file 3−0924. Moreover, the (111) and (200) peaks are also present in TiAlVN/M2 (Fig. 1(c)), indicating that Al and V may dissolve in TiN. The most prominent peak of TiAlN/M2 in Fig. 1(b) may be contributed by the ε (Fe_3N−Fe_2N) phase according to the JCPDS files. The strong peak combined with the numerous related weak peaks may have occurred because of the Fe-containing phases in the nitride coatings, which were not observed in previous studies of TiAlN/M2.

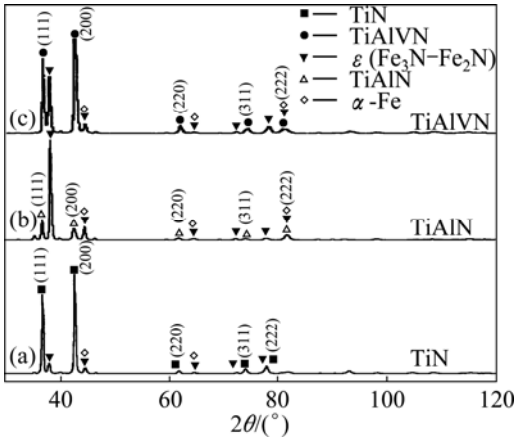

Fig. 1 XRD patterns of TiN/M2, TiAlN/M2 and TiAlVN/M2

Furthermore, the lattice constants were measured by extrapolation. The values of the lattice constant calculated from the diffraction peaks are plotted against $\cos^2\theta/\sin\theta+\cos^2\theta/\theta$, and the straight line is extrapolated to zero; thus, the exact lattice constant (a_0) can be obtained. Data for the TiN, TiAlN, and TiAlVN are shown in Fig. 2. The aluminum-containing nitride films evidently have a smaller lattice constant, but the addition of vanadium to TiAlN increases the lattice constant of the TiAlN coatings.

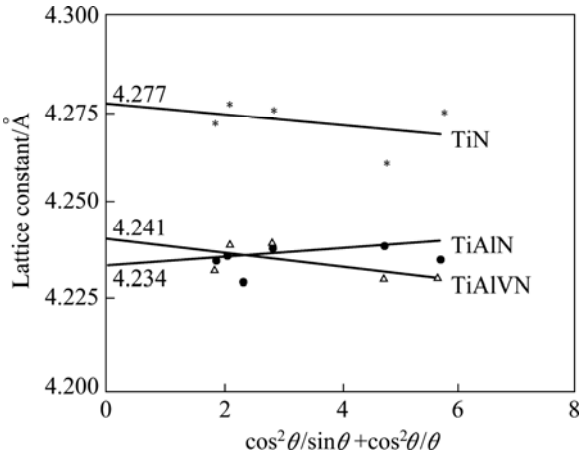

Fig. 2 Extrapolation of measured lattice parameters of TiN, TiAlN and TiAlVN coating versus $\cos^2\theta/\sin\theta+\cos^2\theta/\theta$

3.3 SEM

The cross-sectional SEM morphologies of the TiN, TiAlN and TiAlVN coatings on M2 steel are shown in Fig. 3. It indicates that the columnar structure of TiN/M2 is coarser than that of TiAlN/ M2 or TiAlVN/M2.

3.4 TEM

Figure 4 shows the cross-sectional TEM micrograph of TiN/M2. Moreover, the selected-area diffraction

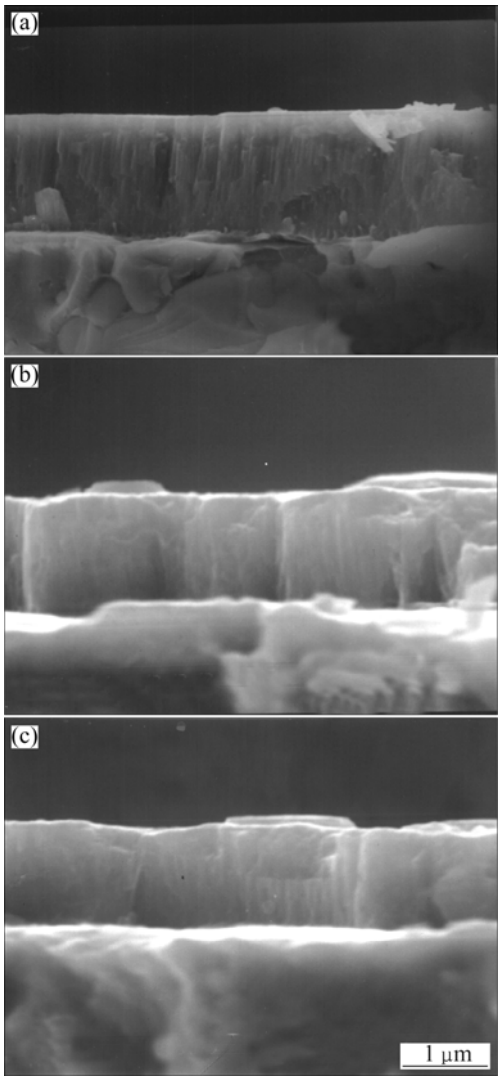

Fig. 3 Cross-sectional SEM micrographs of TiN (a), TiAlN (b), and TiAlVN (c)

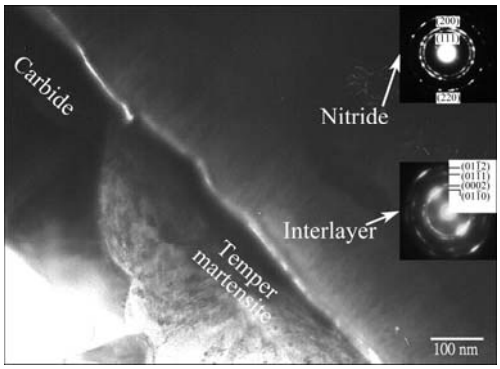

Fig. 4 Cross-sectional TEM micrograph of TiN/M2

(SAD) ring patterns of the nitride and interlayer are also shown in Fig. 6. The preferred orientation for the SAD ring pattern of the interlayer appears as broad intense spots. The thickness of the interlayer ranges between 150 and 200 nm, and the total film thickness is approximately 1.8−2.0 μm.

Figure 5(a) shows the cross-sectional TEM micrograph of TiAlN/M2. An interlayer-separating nitride and substrate are shown in Fig. 5(a) in a similar manner to Fig. 4. Figure 5(b) shows the bright field image (BFI) of the cross-sectional nitride layer, and the SAD ring pattern indicates that this nitride layer is TiAlN. Moreover, the broad spots present in these rings by texture and several other contributions such as the $\varepsilon(Fe_3N-Fe_2N)$ phase are shown on the XRD pattern in Fig. 1(b). The dark field image (DFI) from the (111) SAD ring indicates that the TiAlN layer has the texture structure shown in Fig. 5(c). The SAD ring pattern (Fig. 5(d)) from the interlayer in Fig. 5(a) indicates that the interlayer comprises a TiAl phase. Moreover, the DFI by the SAD $\{01\bar{1}0\}$ spots of the TiAl phase shows the texture microstructures of the interlayer (Fig. 5(d)).

Figure 6(a) shows the cross-sectional TEM micrograph of TiAlVN/M2. Figure 6(b) shows the BFI of the interlayer, which indicates that the interlayer is a texture structure. Furthermore, Fig. 6(b) shows the SAD ring obtained from the interlayer near the interlayer/substrate interface (Fig. 6(a)). The SAD ring pattern indicates a stronger preferred orientation and a slightly larger *d*-spacing (or smaller radius of diffraction rings) compared with those obtained from the interlayer of TiN/M2 and TiAlN/ M2. The larger *d*-spacing may result from dissolving more elements, such as Al, V, and other elements from the substrate (e.g., C) [17]. Figure 6(c) shows the SAD ring pattern obtained from the TiAlVN phase in Fig. 6(a), which shows the same preferred orientations as TiAlN. The corresponding DFI formed by the SAD {111} spots in Fig. 6(c) shows the same type of texture structure as TiAlN. Furthermore, the lattice image of HRTEM in Fig. 6(d) shows a crystallographic relationship of $(01\bar{1}0)_{TiAlV}//(110)_{T.M}$ between the TiAlV phase and the tempered martensite of the substrate.

4 Discussion

4.1 Growth of nitride coatings

The important parameters in the coating growth are sputtering yielding, ion-energy threshold (threshold energy necessary to bombard the target), and scattering within the plasma. The sputtering yield is the number of atoms ejected from the target per incident ion, and is dependent on not only the characteristics of the target material, but also the incident ion energy and mass. The ion-energy threshold is related to the penetration depth of the ions. Together with the heat of the sublimation of the target material, they determine the energy range of the ejected atoms from several tenths of an electron volt up to nearly the full energy of the ions impinging on the target [5]. The energies of the ejected Ti, Al, and V

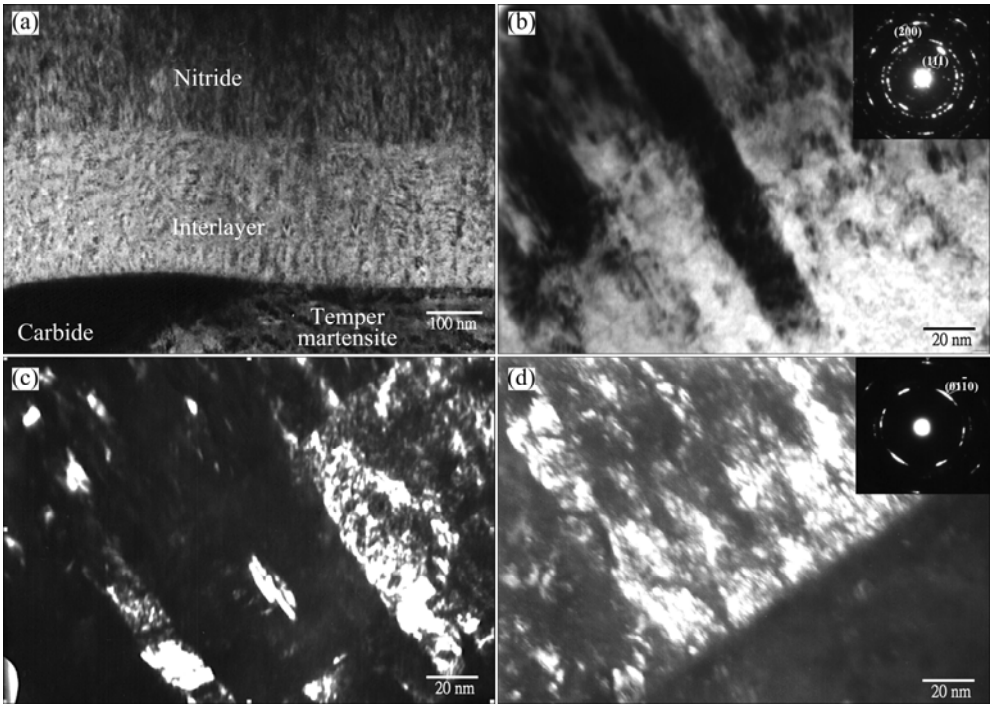

Fig. 5 Cross-sectional TEM micrographs and diffraction patterns of TiAlN/M2: (a) Cross-sectional image; (b) BFI of TiAlN coating; (c) DFI formed from (111) ring in (b); (d) DFI formed from $(01\bar{1}0)$ ring

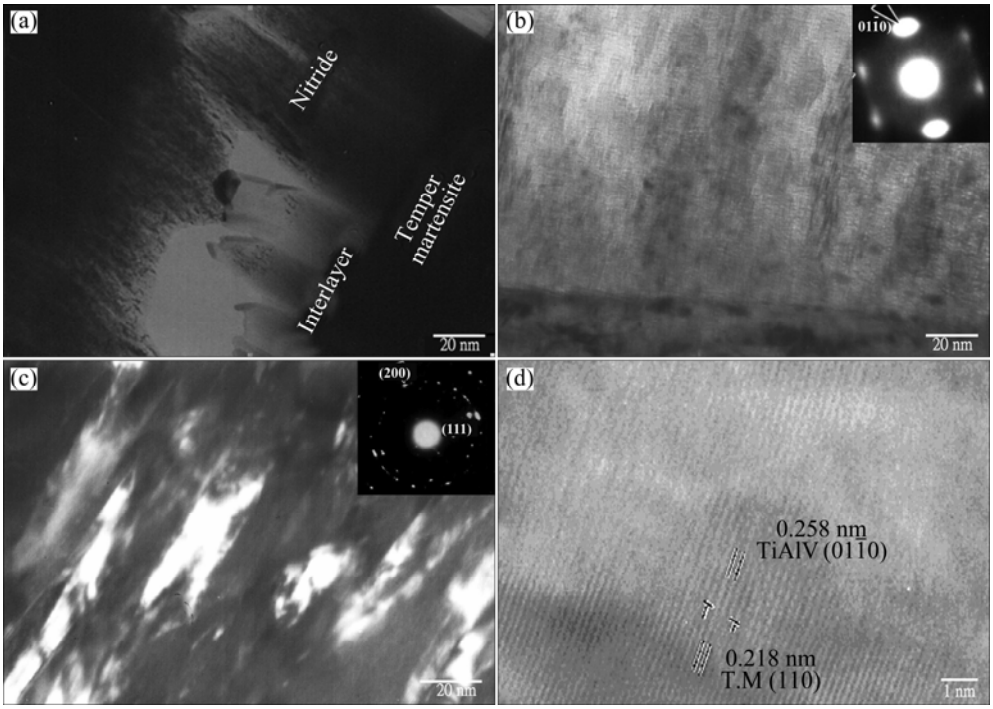

Fig. 6 Cross-sectional TEM micrographs and diffraction patterns of TiAlVN/M2: (a) Cross-sectional image; (b) BFI of interlayer beside interlayer/tempered martensite interface of TiAlVN/ M2; (c) DFI formed from (111) ring; (d) HRTEM image of TiAlVN/ M2 showing orientation relationship and misfit dislocation

atoms by 120 eV Ar bombardment are nearly the same (Ti≥V≥Al=15 eV) [6]. Regarding the effects of the scattering within the plasma, atoms may change their course and arrive at the substrate with lower energies, reducing the deposition rate. In particular, the mean free path varies as the following equation [18]:

$$L = 1/(\sqrt{2}\,\pi a^2 n) \quad (1)$$

where a is a collision cross-section that is proportional to the atomic radius, and n is the number of atoms per volume at the specific temperature and pressure. The Ti, Al, and V atoms sputtered from the target with different

sputtering yields and mean free paths may cause different growth morphologies of the thin films. The sputtering yields at 500 eV for Ti, Al, and V are 0.51, 1.05, and 0.65, respectively [19]. Moreover, the atomic radii for Ti, Al, and V are 0.147 nm, 0.143 nm, and 0.133 nm, respectively [20]. Furthermore, the multicomponent cathode has a higher deposition rate than a pure Ti, pure Al, or pure V cathode. A spectrometrical analysis indicates that the alloyed targets generally favor the emission of more particles with higher energy and suppress the emission of macro-particles. Therefore, the incorporation of Al in the Ti target may improve the coarse columnar structure of TiN mononitride (Fig. 3(a)) in addition to the thermal stability benefit because of the smaller radius, higher sputtering yield, and higher diffusion coefficient of Al. The denser and more fibrous columnar structure of TiAlN coatings (Fig. 3(b)) corresponds to the ZT mode of Thornton's structure model, which is better than the Z1 mode with voids for TiN [21]. Moreover, the growth morphology for TiAlVN films (Fig. 3(c)) corresponds to the ZT mode because of the larger mean free path of V atoms.

The benefit of a denser and finer columnar structure is reflected in the improvement of the surface smoothness and mechanical properties such as hardness. The TiAlVN and TiAlN coatings are smoother than the TiN films, and the TiAlVN coating has the highest hardness of HV1690 among them in this study, which is consistent with previous studies of TiVN [14] and TiAlVN [17].

4.2 Microstructure of nitride coatings

Hagg's model indicates that the transition metal and interstitial elements may form stable structures under the condition that the ratio of their atomic radius is less than 0.59, and the metal substructure may not remain the same (e.g., from hcp to fcc for Ti). The N/Ti radius ratio of 0.457 suggests that TiN can be stable with the NaCl (B1) structure. The lattice constant of TiN changes with the N concentration, which can be expressed as [18,22]

$$a(\pm 0.0002) = 0.4415 - 0.000348N \ (N>50\%) \quad (2)$$

$$a(\pm 0.0002) = 0.4159 + 0.000164N \ (N<50\%) \quad (3)$$

Equations (2) and (3) give the relationships between the lattice constant a and nitrogen mole concentration N. The lattice constant of the monocell TiN in this study is approximately 0.427 nm, which changes in TiAlN and TiAlVN coatings, as shown in Fig. 2. These shifts are related to the concentrations and types of substitutional elements. The lattice constant decrease of the TiAlN phase is primarily due to the smaller Al atoms. However, the lattice constant of TiAlVN is larger than that of TiAlN, and the bonding characteristics of each element with nitride atoms may be involved, in addition to the atomic radius in this case. The bonding of Ti and V with N is metallic, but that of Al is covalent. The ionic radii are 0.076, 0.057, and 0.061 nm for Ti^{3+}, Al^{3+} and V^{3+}($V^{3+}>Al^{3+}$), respectively. Moreover, the atomic radii are 0.147, 0.143, and 0.133 nm for Ti, Al, and V, respectively [20]. Therefore, the addition of V to TiAlN films may reduce the difference of the lattice constants relative to the monocell TiN phase (Fig. 2), which is in agreement with the study regarding the dimensional stability of V in multicomponent Ti-based nitride films [17].

Figure 6(d) shows the corresponding lattice image, and the crystallographic relationship is $(01\bar{1}0)_{TiAlV}//(110)_{T.M}$ with misfit dislocations indicated in the figure. Another orientation relationship of $(110)_{\alpha-Fe}//(110)_{TiFe}//(1100)_{\alpha-Ti}$ at the interface of TiN/M2 was discovered by WEN et al [23]. However, the lattice structure of α-Fe is similar to that of TiFe, and Fig. 6(b) shows the SAD ring pattern in the interlayer beside the interlayer/tempered martensite interface, indicating the strongest diffraction (first ring) contributed by α-Ti containing Al, V, and other elements such as C from the substrate. Therefore, the orientation relationship observed by WEN et al [23] is reasonable. The misfit (δ) between the two lattices is 0.21 nm, and the Burgers (b) vector is approximately 1.083 nm ($D\cong b/\delta$, $b=a_\alpha+a_\beta/2$ [24]), so that there is an edge dislocation every five (110) lattice spacings ($D \cong 1.083/0.21 \cong 5.1$), as shown in Fig. 6(d).

Regarding the nitride phase in the outer zone, major diffractions from the (111) and (200) planes with minor variations between the major two orientations are all shown in Figs. 4, 5(b), and 6(c) from TiN/M2, TiAlN/ M2, and TiAlVN/ M2, respectively. PELLEG et al [25] proposed that the preferred orientation is determined by whether the strain energy or surface energy is the dominant factor during the growth of the coatings. In general, the (200) preferred orientation often appears with decreased surface energy when the surface energy is the dominant factor. However, there is ambiguity in the preferred (111) orientation of this model. Therefore, theories based on Einstein's theory of Brownian motion and Eyring's transition state model have been used to analyze the preferred orientations of film growth and the condensation and coalescence of nanocrystals [11,13]. The non-epitaxy crystallite from the model can rotate between the (200) and (111) orientations by an external electric field and thermally activated rotation.

5 Conclusions

1) The addition of Al into TiN of the lattice constant reduces its lattice constant from 0.4277 to 0.4234 nm, but a further addition of V increases it to 0.4241 nm.

2) The columnar structure of TiN/M2 is coarser than

that of TiAlN/M2 or TiAlVN/M2, and TiAlVN/M2 has the highest hardness of HV1690 among the three coatings.

3) The interlayers of TiN/M2, TiAlN/M2, and TiAlVN/M2 have preferred $[01\bar{1}0]_{\alpha\text{–Ti}}$, $[01\bar{1}1]_{\sigma\text{–Ti}}$, and $[0002]_{\sigma\text{–Ti}}$ orientations, but those of TiAlVN/M2 are stronger than the others.

4) The nitride films of TiAlN/M2 and TiAlVN/M2 have preferred (110) and (200) orientations. Moreover, the preferred orientation of $(100)_{\varepsilon(Fe_3N–Fe_2N)}$ is also present in TiAlN/M2.

5) The interface between the α-Ti interlayer and tempered martensite of TiAlVN/M2 has a $(01\bar{1}0)_{\alpha\text{–Ti}}$// $(110)_{T.M}$ orientation relationship. Moreover, misfit dislocations are present.

References

[1] CHO D H, LEE Y Z. Evaluation of fing surfaces with several coatings for friction wear and scuffing life [J]. Transactions of Nonferrous Metals Society of China, 2009, 19(4): 992−996.

[2] CHAKRABRTI K, JEONG J J, HWANG S K, YOO Y C, LEE C M. Effects of nitrogen flow rates on the growth morphology of TiAlN films prepared by an rf-reactive sputtering technique [J]. Thin Solid Films, 2002, 406: 159−163.

[3] ZHAO H, WANG X H, LIU Q L, CHEN L J, LIU Z. Structure and wear resistance of TiN and TiAlN coatings on AZ91 alloy deposited by multi-arc ion plating [J]. Transactions of Nonferrous Metals Society of China, 2010, 20(S2): s679−s682.

[4] CHIEN C C, LIU K T, DUH J G, CHANG K W, CHUNG K H. Effect of nitride film coatings on cell compatibility [J]. Dental Materials, 2008, 24: 986−993.

[5] SCHAFFER E, KLEER G. Mechanical behavior of (Ti,Al)N coatings exposed to elevated temperatures and an oxidative environment [J]. Surface and Coatings Technology, 2000, 133−134: 215−219.

[6] BARSHILIA H C, RAJAM K S, JAIN A, GOPINADHAN K, CHAUDHARY S. A comparative study on the structure and properties of nanolayered TiN/N_bN and TiAlN/TiN multilayer coatings prepared by reactive direct current magnetron sputtering [J]. Thin Solid Films, 2006, 503: 158−166.

[7] BOBZIN K, LUGSCHEIDER E, MAES M, IMMICH P, BOLZA S. Grain size evaluation of pulsed TiAlN nanocomposite coatings for cutting tools [J]. Thin Solid Films, 2007, 515: 3681−3684.

[8] TILLMANN W, VOGLI E, MOMENI S. Mechanical and tribological properties of Ti/TiAlN duplex coatings on high and low alloy tool steels [J]. Vacuum, 2010, 84: 387−392.

[9] ANANTHAKUMAR R, SUBRAMANIAN B, KOBAYASHI A, JAYACHANDRAN M. Electrochemical corrosion and materials properties of reactively sputtered TiN/TiAlN multilayer coatings [J]. Ceramics International, 2012, 38: 477−485.

[10] DU H, ZHAO H B, XIONG J, XIAN G. Effect of interlayers on the structure and properties of TiAlN based coatings on WC−Co cemented carbide substrate [J]. International Journal of Refractory Metals and Hard Materials，2013, 37: 60−66.

[11] RAVEH A, ZUKERMAN I, SHNECK R, AVNI R, FRIED I. Thermal stability of nanostructured superhard coatings [J]. Surface and Coatings Technology, 2007, 201: 6136−6142.

[12] LUO Q S, WANG S C, ZHOU Z X, CHEN L H. Structure characterization and tribological study of magnetron sputtered nanocomposite nc-TiAlV(N,C)/a-C coatings [J]. Journal of Materials Chemistry, 2011, 21: 9746−9756.

[13] LUO Q, HOVSEPIAN P E. Transmission electron microscopy and energy dispersive X-ray spectroscopy on the worn surface of nano-structured TiAlN/VN multilayer coating [J]. Thin Solid Films, 2006, 497: 203−209.

[14] ZHOU Z, RAINFORTH W M, LUO Q, HOVSEPIAN P E, OJEDA J J, ROMERO-GONZALEZ M E. Wear and friction of TiAlN/VN coatings against Al_2O_3 in air at room and elevated temperatures [J]. Acta Materialia, 2010, 58: 2912−2925.

[15] MAYRHOFER P H, HOVSEPIAN P E, MITTERER C, MÜNZ W D. Calorimetric evidence for frictional self-adaptation of TiAlN/VN superlattice coatings [J]. International Conference on Metallurgical Coatings and Thin Films, 2004, 177−178: 341−347.

[16] RAMADOSS R, KUMAR N, PANDIAN R, DASH S, RAVINDRAN T R, ARIVUOLI D, TYAGI A K. Tribological properties and deformation mechanism of TiAlN coating sliding with various counterbodies [J]. Tribology International, 2013, 66: 143−149.

[17] FRANZ R, MITTERER C. Vanadium containing self-adaptive low-friction hard coatings for high-temperature applications: A review [J]. Surface and Coatings Technology, 2013, 228: 1−13.

[18] SMITH D. Thin–film deposition principles and practice [M]. New York: McGraw-Hill Professional, 1999: 23−24.

[19] RICKERBY D S, MATTHEWS A. Advanced surface coatings: A handbook of surface engineering [M]. London: Blackie and Son, 1991: 96−97.

[20] SCHAFFER J T, SAXENA A, ANTOLOVICH S D, SANDERS T H, WARNER S B. The science and design of engineering materials [M]. New York: Magraw-Hill Book Company, 1999: 77−79.

[21] THORNTON J A. Influence of apparatus geometry and deposition conditions on the structure and topography of thick sputtered coatings [J]. Journal of Vacuum Science and Technology, 1974, 11(4): 666−670.

[22] RIBEIRO E, MACLCZYK A, CARVALHO S, REBOUTA L, FERNANDERS J V, ALEVES E, MIRANDA A S. Effects of ion bombardment on properties of DC sputtered superhard (Ti,Si,Al)N nanocomposite coatings [J]. Surface and Coatings Technology, 2002, 151−152: 515−520.

[23] WEN L S, JIANG X, SI C Y. A transmission electron microscopy study on Ti−N films deposited by ion plating [J]. Journal of Vacuum. Science Technology A, 1986, 4(6): 2682−2687.

[24] PORTER D A, EASTERLING K E, SHERIF M Y. Phase transformation in metals and alloys [M]. London: Taylor & Francis Group, 2009: 145−148.

[25] PELLEG J, ZEVIN L Z, LUNGO S, CROITORU N. Reactive-sputter-deposited TiN films on glass substrates [J]. Thin solid films, 1991, 197(1−2): 117−128.

AISI M2 钢上磁控溅射 TiN、TiAlN 和 TiAlVN 薄膜的显微结构

王翠凤[1]，欧士辅[2]，邱锡荣[2]

1. 福建信息职业技术学院 机电工程系，福州 350003；
2. 高雄应用科技大学 模具工程系，高雄 80706

摘 要：为了研究 Al 和 V 掺杂对 TiN 薄膜微结构的影响，用磁控溅射法在 AISI M2 高速钢上沉积 TiN、TiAlN 和 TiAlVN 薄膜。采用 XRD、SEM 和 TEM 对薄膜的显微结构进行表征。结果表明，TiN 薄膜中掺杂 Al 引起了晶格常数的降低，TiAlN 中掺杂 V 则导致晶格常数的增加。另外，TiN、TiAlN 和 TiAlVN 薄膜的生长形态显示，添加 Al 和 V 有改善柱状结构的倾向。在 TiN、TiAlN 和 TiAlVN 薄膜中鉴定出(111)和(200)晶向，$\varepsilon(Fe_3N-Fe_2N)$相的存在是因为薄膜中存在少量的 Fe。TiAlN 和 TiAlVN 薄膜夹层具有 $(01\bar{1}0)$ 择优取向。在 TiAlN 和 TiAlVN 薄膜中观察到(111)和(200)晶向的织构(柱状)结构，在 TiAlVN/M2 夹层和回火马氏体之间存在 $(01\bar{1}0)_{\alpha-Ti}//(110)_{T.M}$ 的位向关系。

关键词：薄膜；TiAlVN 薄膜；溅射率；晶向关系

(Edited by Xiang-qun LI)